Supporting Information

Bias-induced surface reconstruction of MOF-derived bimetallic (Co &V) oxide as an electrocatalyst for water oxidation

Malaya K. Sahoo[a,b], Nisarani Bishoyi[a,b], Deepak K. Swain[a,b], J. N. Behera[a,b]*

[a]National Institute of Science Education and Research (NISER) an OCC of HBNI, Bhubaneswar, Khurda, Odisha, India,752050.

[b]Centre for Interdisciplinary Sciences (CIS), NISER, Khurda, Odisha, India, 752050

Email: jnbehera@niser.ac.in

Electrochemical Calculations:

All electrochemical measurements are recorded taking Hg/HgO as the reference electrode and converted to a reversible hydrogen electrode (R.H.E) using the following equation for data presentation.

$$E_{RHE} = E^{\circ}_{Hg/HgO} + 0.059 \times pH + E_{Hg/HgO}$$

iR compensation has been done using the following equation to describe the intrinsic performance of the catalysts which has been suppressed by the suppressed and contact resistance.[1]

$$E_{iR} = E - iR$$

Mass activity: The obtained current from linear sweep voltammograms is normalized w.r.t the loaded mass and plotted against the working electrode potential in the RHE scale. Here 1 mg of sample is dispersed in 95 µL of ethanol and the 5µL of Nafion and 5 µL of the catalyst ink were dropcasted on the GCRDE electrode. Thus it assumed that 0.05 mg of sample was loaded for the evaluation of the mass activity.

Turn Over Frequency:

The number of moles of cobalt and vanadium present per mg of annealed products was calculated from ICP-OES and from there the moles of metals in 0.05 mg of sample were

calculated and after that turn-over frequency (TOF) was calculated following the equation given below considering all the cobalt sites are participating in the catalysis process.

$$TOF = \frac{J \times S}{4 \times F \times n}$$

Where 'J' corresponds to the current density obtained from LSV, 'S' corresponds to the geometrical surface area of the GCRDE working electrode, 'F' corresponds to the faraday constant, and 'n' refers to the number of moles of cobalt present in the loaded sample and 4 is dived since OER follows a four-electron pathway.[2]

Faradic efficiency:

The efficiency of the CoV@600 towards the catalysis of oxygen evolution reaction was quantified from faradic efficiency. In order to get the efficiency, LSV was recorded at 5 mV/S within a potential range of 0.0 to 0.8 V w.r.t Hg/HgO reference electrode. The working electrode here used has a glassy carbon disk coated with the catalyst for the water oxidation and platinum ring for the reduction of evolved oxygen and rotates at 1600 rpm. A constant potential of -0.5 V has been applied to the platinum ring to get the oxygen reduction reaction (ORR) current. The following equation is used to evaluate the efficiency of the OER catalyst at 1.5 V (RHE).

$$Faradic\ Efficiency = \frac{I_{Ring} \times n_D}{I_{Disk} \times n_R \times N_{CL}}$$

Where I_{Ring} and I_{Disk} are the current obtained from the platinum ring and glassy carbon disk respectively. Here nR and nD are the number of electron pathways followed by both process and in this case, both OER and ORR follows a four-electron pathway. N_{CL} refers to the collection efficiency of the RRDE electrode used here which has a collection efficiency of 0.249.[3]

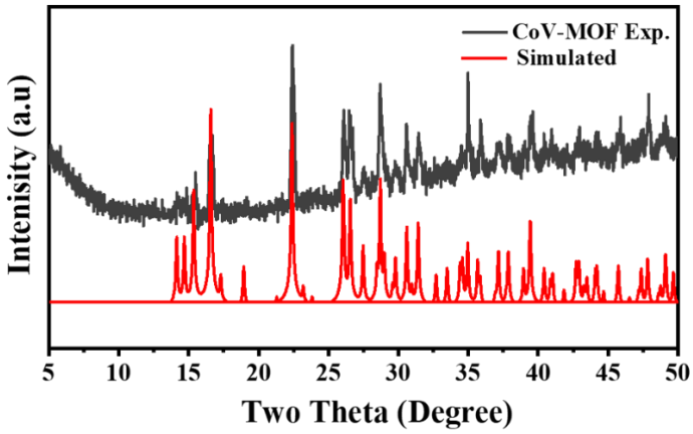

Figure S1 Simulated and experimental powder diffraction pattern of the as-synthesized MOF.

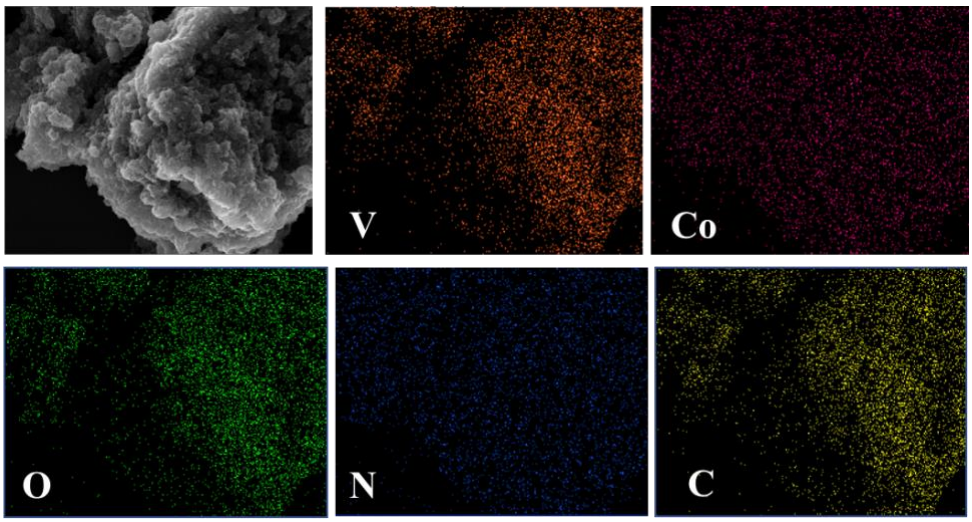

Figure S2a Elemental mapping of CoV-MOF annealed at 600 ˚C.

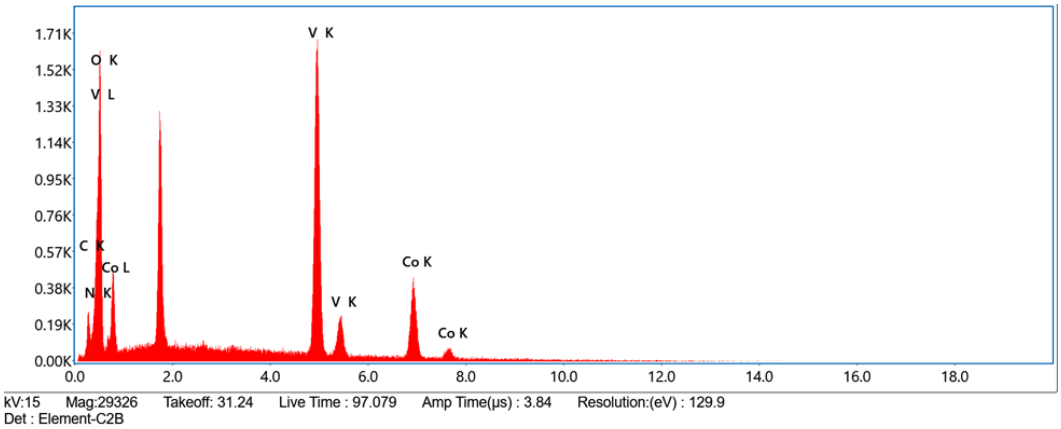

Figure S2b EDAX spectrum of CoV-MOF annealed at 600 ˚C.

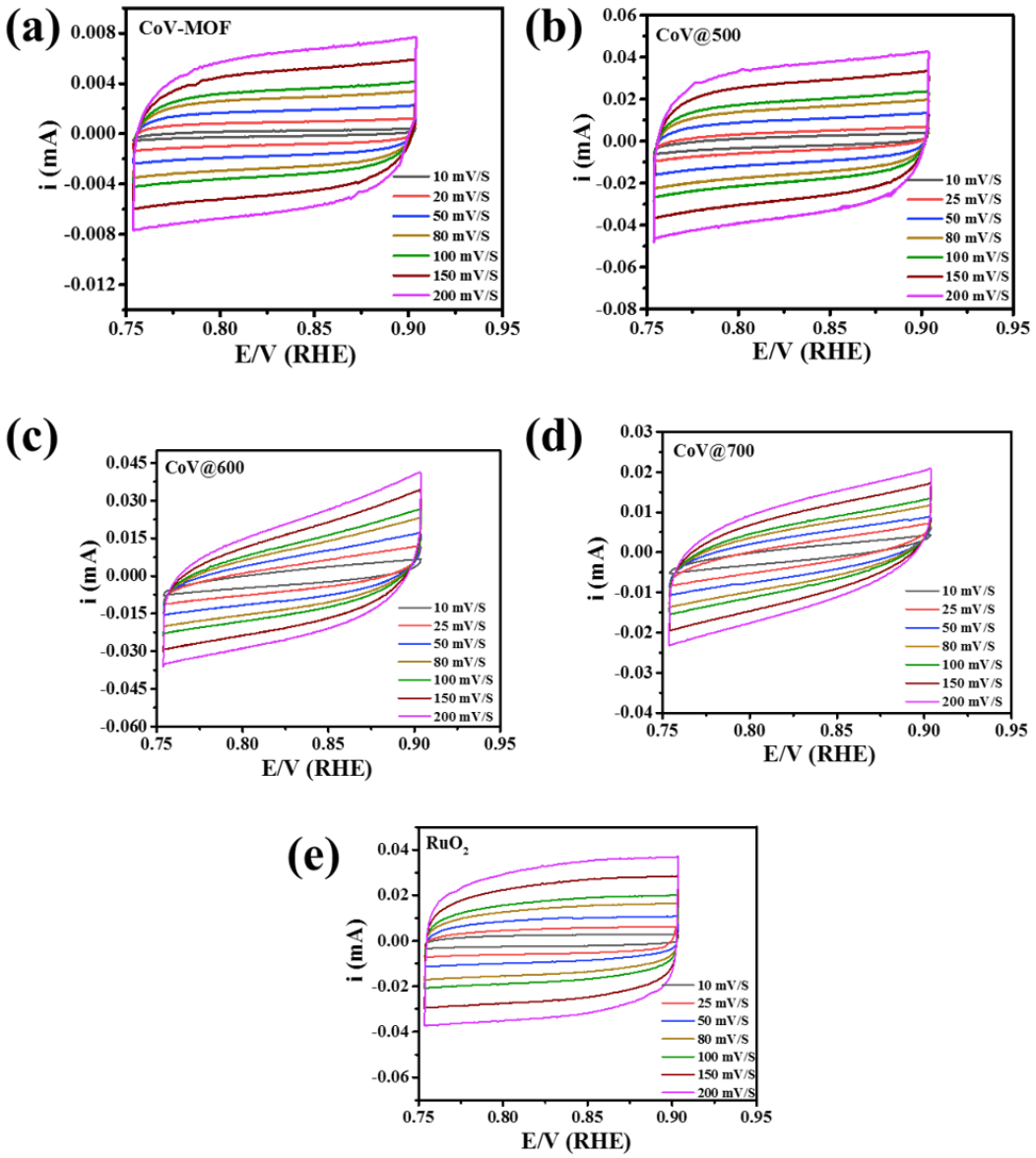

Figure S3 Cyclic Voltammetry at different scan rates of all the catalysts.

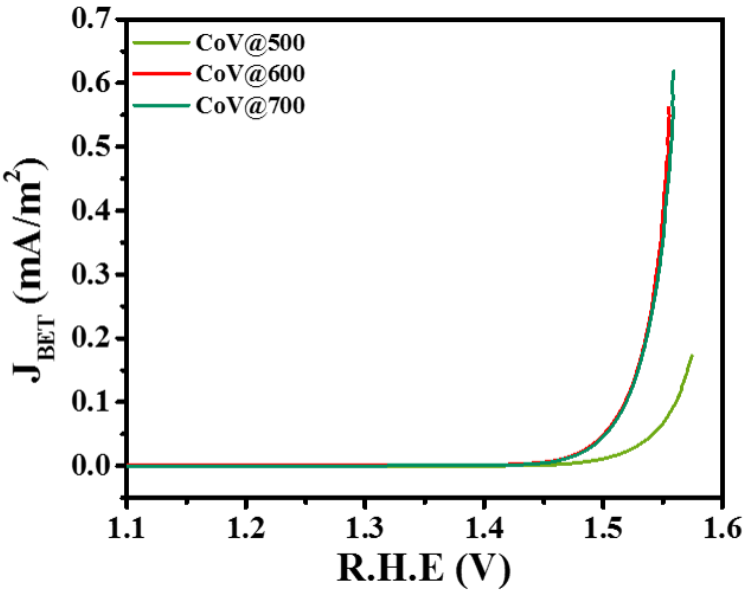

Figure S4 Linear sweep voltammograms of the annealed products normalized with BET surface area.

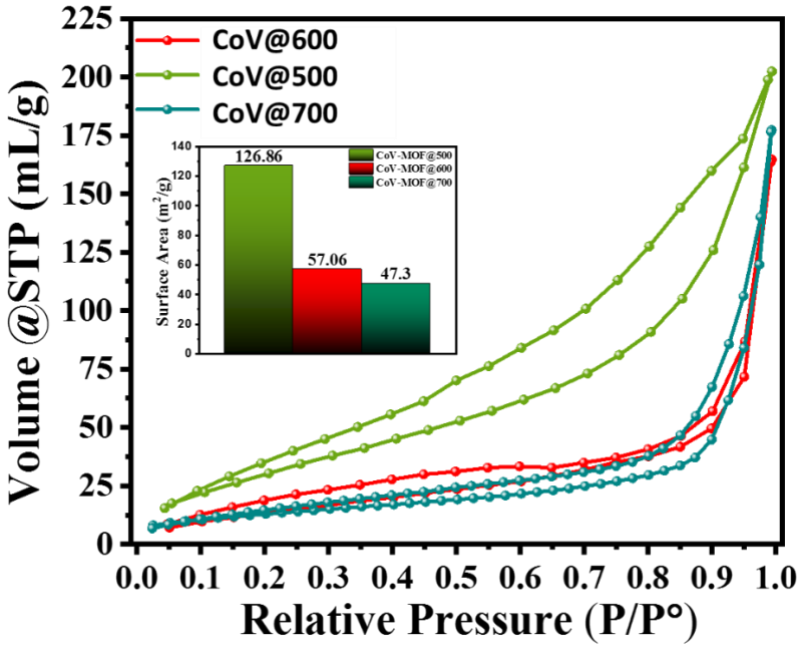

Figure S5 Post-OER N_2 sorption of all the annealed products.

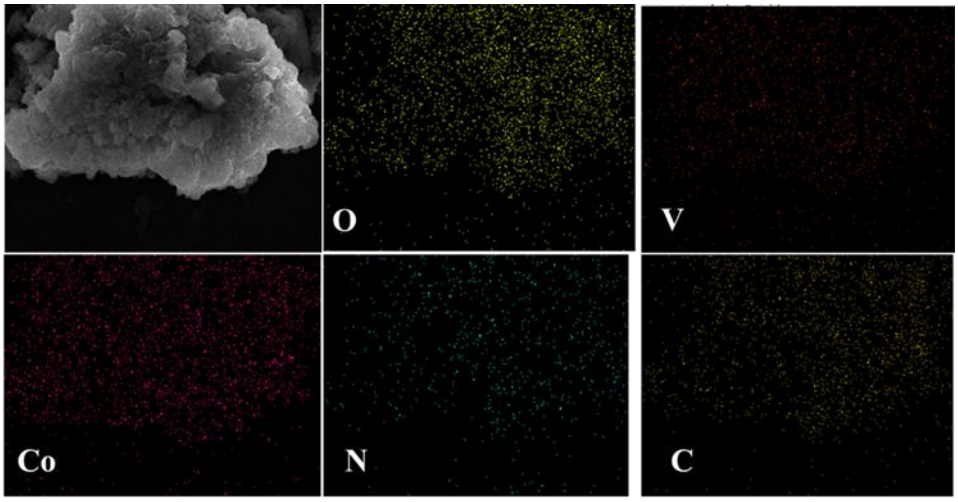

Figure S6 Post-OER elemental mapping of CoV@600.

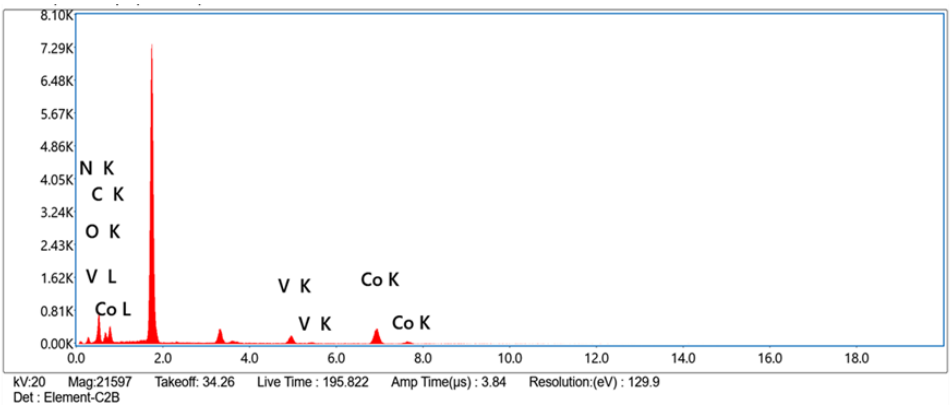

Figure S7 EDAX spectrum of the CoV@600 after catalysis.

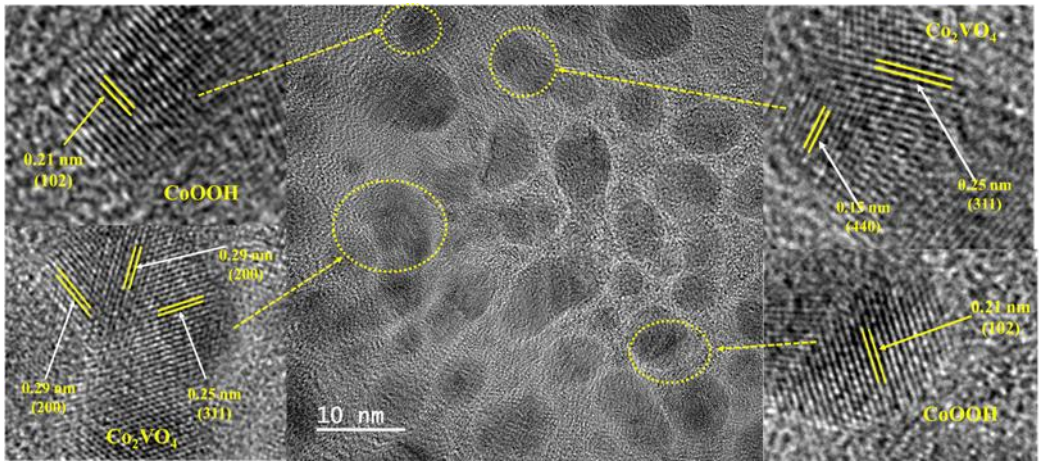

Figure S8 Post-OER HRTEM analysis of the CoV@600 confirming the presence of both Co_2VO_4 and CoOOH.

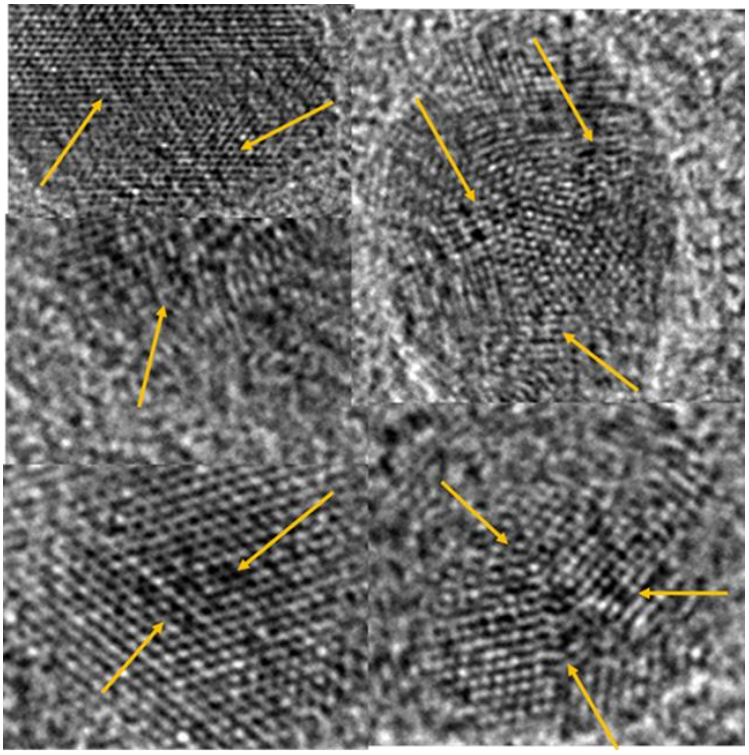

Figure S9 Presence of defects in CoV@600 after OER catalysis.

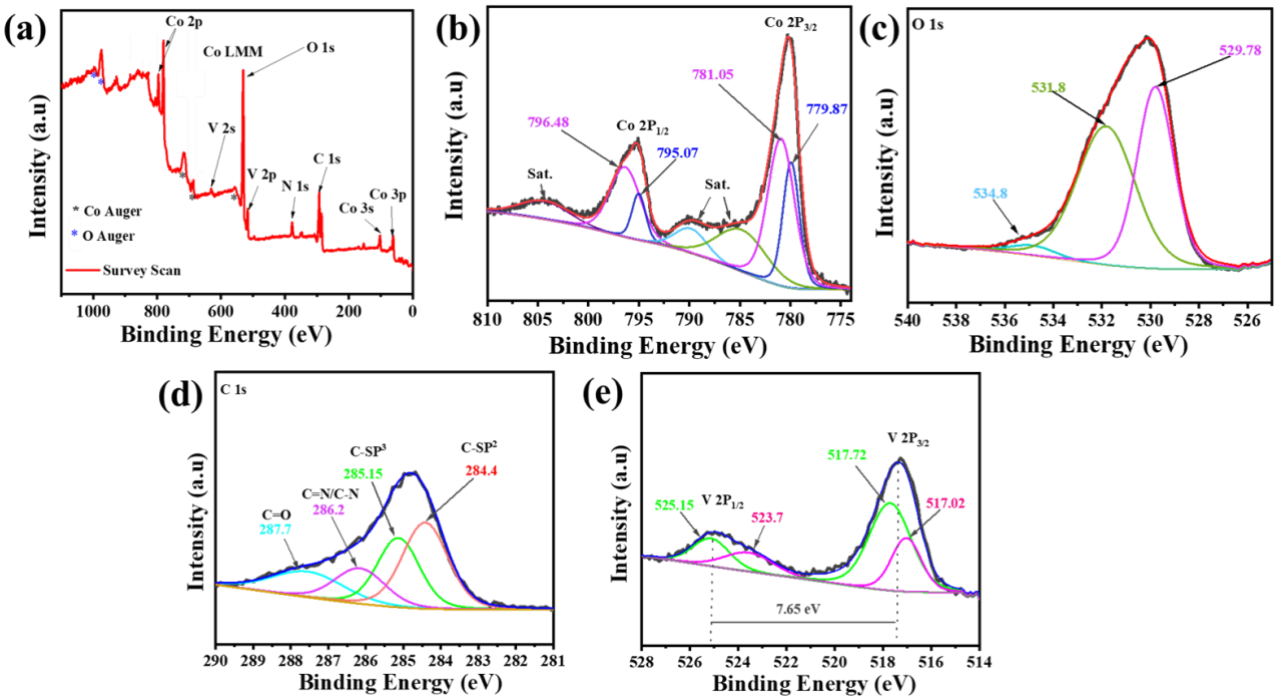

Figure S10 X-Ray photoelectron spectroscopy of CoV@600 after catalysis.

Table S1 Elemental analysis from the EDAX spectrum of the CoV@600

Element	Weight %	Atomic %	Error %	Net Int.
C K	3.60	11.00	13.30	13.00
N K	2.40	6.30	13.60	12.00
O K	11.40	26.10	13.20	31.20
V K	52.70	38.00	2.80	220.10
Co K	29.90	18.60	5.10	59.70

Table S2 Electrochemical OER performance of all the catalysts.

Catalyst	Onset $\Delta\eta$ (mV)	$\Delta\eta$ (mV) @10 mA/cm^2	ECSA (cm^2)	Roughness Factor	Charge-transfer resistance (R_{CT})	Mass Activity (A/g)	Turn-Over Frequency (S^{-1})
CoV-MOF	343 mV	404 mV	0.7975	11.392	141	2.1	0.75
CoV@500	247 mV	288 mV	4.437	63.3857	87	18	4.8
CoV@600	234 mV	273 mV	2.625	37.5	53	35	7.7
CoV@700	242 mV	279 mV	1.55	22.143	72	24	5.2
RuO_2	274 mV	326 mV	4.037	57.67	58	7.2	1.5

Table S3 ICP-OES metal content analysis of the annealed samples

Catalyst	Amount of cobalt (µmol/mg)	Amount of vanadium (µmol/mg)	The ratio of cobalt to vanadium	µmol of cobalt loaded on the electrode	µmol of vanadium loaded on the electrode
CoV-MOF	3.813	7.64	1:2	0.19	0.382
CoV@500	4.41	8.8131	1:1.998	0.22	0.44
CoV@600	4.715	9.417	1:1.9973	0.235	0.471
CoV@700	4.847	9.681	1:1.99732	0.242	0.484

Table S4 Post-OER CoV@600 elemental composition from EDAX

Element	Weight %	Atomic %	Error %	Net Int.
C K	11.80	25.30	13.90	4.50
N K	0.40	0.70	97.80	0.20
O K	29.40	47.30	10.80	19.50
V K	12.10	6.10	5.70	13.10
Co K	45.70	20.00	3.50	28.90

Table S5 ICP-OES metal content analysis of the annealed products after catalysis

Catalyst	µmols of cobalt leached into the electrolyte	µmols of vanadium leached into the electrolyte	% of vanadium leached	% of cobalt leached
CoV@500	0.0122	0.349	79.3	5.54
CoV@600	0.00966	0.333	70.76	4.11
CoV@700	0.00865	0.3292	68.01	3.57

Table S6 Table of comparison of some of the recently reported materials with the present work

OER electrocatalyst	Overpotential (mV)	Tafel slope (mV/decade)	Electrolyte	References
V-Co-Fe-343	307	36	1.0 M KOH	[4]
m-$CoVO_x$	358	63	1.0 M KOH	[5]
Co-B@Co-Bi	291	120.73	1.0 M KOH	[6]
CoNi-P-3DHFLM	292	84	1.0 M KOH	[7]
$CoVO_x$-300	330	46	1.0 M KOH	[8]
CV(1:1)	194	20	1.0 M KOH	[9]
NF@$Co_{0.76}V_{0.25}$-HNNs	268	80	1.0 M KOH	[10]
Co-Fe-B/NF	270@50mA	36	1.0 M KOH	[11]
B doped CoO-Ov/GC	280	71	1.0 M KOH	[12]
B doped $NiFe_2O_4$	271.3	42.08	1.0 M KOH	[13]
$CoFe_{0.2}S_x$	320	48.7	1.0 M KOH	[14]
CFO-RH400	230	68.7	1.0 M KOH	[15]
Co-Co_3O_4@NC-4	260	88	1.0 M KOH	[16]
CoVFeN@NF	212	34.8	1.0 M KOH	[17]
CoNS/C	345	83.3	0.1 M KOH	[18]
$Co_3(VO_4)_2$-II	330	59	1.0 M KOH	[19]

$CoV_{1.5}Fe_{0.5}O_4$	300	38	1.0 M KOH	[20]
Co-UH	250	60	1.0 M KOH	[21]
$Co_{0.8}V_{0.2}OOH$	190	39.6	1.0 M KOH	[22]
H_2O-Plasma Exfoliated CoFe-LDH	232	36	1.0 M KOH	[23]
Ni2V-MOFs@NF	244	38.1	1.0 M KOH	[24]
CoV-MOF	404	81.11	1.0 M KOH	This Work
CoV@500	288	59.8		
CoV@600	273	54.32		
CoV@700	279	53.75		

References:

(1) Anantharaj, S.; Noda, S. IR Drop Correction in Potentiostatic Electrocatalysis: Everything One Needs to Know! *J. Mater. Chem. A* **2022**, 9348–9354. https://doi.org/10.1039/D2TA01393B.

(2) Ahmed, Z.; Krishankant; Rai, R.; Kumar, R.; Maruyama, T.; Bera, C.; Bagchi, V. Unraveling a Graphene Exfoliation Technique Analogy in the Making of Ultrathin Nickel-Iron Oxyhydroxides@Nickel Foam to Promote the OER. *ACS Appl. Mater. Interfaces* **2021**, *13* (46), 55281–55291. https://doi.org/10.1021/acsami.1c19536.

(3) Gao, D.; Liu, R.; Liu, S.; Greiner, S.; Anjass, M.; Biskupek, J.; Kaiser, U.; Braun, H.; Jacob, T.; Streb, C. Electrocatalytic Oxygen Evolution by Hierarchically Structured Cobalt-Iron Composites. *ACS Applied Materials and Interfaces*. **2021**, pp 19048–19054. https://doi.org/10.1021/acsami.1c03618.

(4) Gao, T.; Jin, Z.; Liao, M.; Xiao, J.; Yuan, H.; Xiao, D. A Trimetallic V-Co-

Fe Oxide Nanoparticle as an Efficient and Stable Electrocatalyst for Oxygen Evolution Reaction. *J. Mater. Chem. A* **2015**, *3* (34), 17763–17770. https://doi.org/10.1039/c5ta04058b.

(5) Liardet, L.; Hu, X. Amorphous Cobalt Vanadium Oxide as a Highly Active Electrocatalyst for Oxygen Evolution. *ACS Catal.* **2018**, *8* (1), 644–650. https://doi.org/10.1021/acscatal.7b03198.

(6) Tan, T.; Han, P.; Cong, H.; Cheng, G.; Luo, W. An Amorphous Cobalt Borate Nanosheet-Coated Cobalt Boride Hybrid for Highly Efficient Alkaline Water Oxidation Reaction. *ACS Sustain. Chem. Eng.* **2019**, *7* (6), 5620–5625. https://doi.org/10.1021/acssuschemeng.9b00258.

(7) Li, G.; Zhang, X.; Zhang, H.; Liao, C.; Jiang, G. Bottom-up MOF-Intermediated Synthesis of 3D Hierarchical Flower-like Cobalt-Based Homobimetallic Phophide Composed of Ultrathin Nanosheets for Highly Efficient Oxygen Evolution Reaction. *Appl. Catal. B Environ.* **2019**, *249* (February), 147–154. https://doi.org/10.1016/j.apcatb.2019.03.007.

(8) Jiang, C.; Yang, J.; Zhao, T.; Xiong, L.; Guo, Z. X.; Ren, Y.; Qi, H.; Wang, A.; Tang, J. Co3+-O-V4+ Cluster in CoVOx Nanorods for Efficient and Stable Electrochemical Oxygen Evolution. *Appl. Catal. B Environ.* **2021**, *282* (May 2020), 119571. https://doi.org/10.1016/j.apcatb.2020.119571.

(9) Keerthana, S.; Yuvakkumar, R.; Ravi, G.; Pannipara, M.; Al-Sehemi, A. G.; Velauthapillai, D. Cobalt Vanadium Oxide Nanoclusters for Oxygen Evolution Reaction. *ECS J. Solid State Sci. Technol.* **2021**, *10* (7), 071003. https://doi.org/10.1149/2162-8777/ac0e0f.

(10) Yang, M.; Fu, X.; Shao, M.; Wang, Z.; Cao, L.; Gu, S.; Li, M.; Cheng, H.; Li, Y.; Pan, H.; Lu, Z. Cobalt-Vanadium Hydroxide Nanoneedles with a Free-Standing Structure as High-Performance Oxygen Evolution Reaction Electrocatalysts. *ChemElectroChem* **2019**, *6* (7), 2050–2055. https://doi.org/10.1002/celc.201900415.

(11) Patil, K.; Babar, P.; Li, X.; Karade, V.; Kim, S.; Jang, S. Y.; Bhoite, P.; Kim, J. H. Co–Fe–B Nanochain Electrocatalysts for Oxygen Evolution at High Current Density. *ACS Appl. Nano Mater.* **2022**. https://doi.org/10.1021/acsanm.2c00312.

(12) Zhang, K.; Zhang, G.; Qu, J.; Liu, H. Disordering the Atomic Structure of Co(II) Oxide via B-Doping: An Efficient Oxygen Vacancy Introduction Approach for High Oxygen Evolution Reaction Electrocatalysts. *Small* **2018**, *14* (41), 1–9. https://doi.org/10.1002/smll.201802760.

(13) Wei, R.; Bu, X.; Gao, W.; Villaos, R. A. B.; MacAm, G.; Huang, Z. Q.; Lan, C.; Chuang, F. C.; Qu, Y.; Ho, J. C. Engineering Surface Structure of

Spinel Oxides via High-Valent Vanadium Doping for Remarkably Enhanced Electrocatalytic Oxygen Evolution Reaction. *ACS Appl. Mater. Interfaces* **2019**, *11* (36), 33012–33021. https://doi.org/10.1021/acsami.9b10868.

(14) Wang, M.; Dong, C. L.; Huang, Y. C.; Shen, S. Operando Spectral and Electrochemical Investigation into the Heterophase Stimulated Active Species Transformation in Transition-Metal Sulfides for Efficient Electrocatalytic Oxygen Evolution. *ACS Catal.* **2020**, *10* (3), 1855–1864. https://doi.org/10.1021/acscatal.9b05170.

(15) Huang, K.; Zhao, Z.; Du, H.; Du, P.; Wang, H.; Wang, R.; Lin, S.; Wei, H.; Long, Y.; Lei, M.; Guo, W.; Wu, H. Rapid Thermal Annealing toward High-Quality 2D Cobalt Fluoride Oxide as an Advanced Oxygen Evolution Electrocatalyst. *ACS Sustain. Chem. Eng.* **2020**, *8* (18), 6905–6913. https://doi.org/10.1021/acssuschemeng.0c00830.

(16) Guo, Q.; Mao, J.; Huang, J.; Wang, Z.; Zhang, Y.; Hu, J.; Dong, J.; Sathasivam, S.; Zhao, Y.; Xing, G.; Pan, H.; Lai, Y.; Tang, Y. Reducing Oxygen Evolution Reaction Overpotential in Cobalt-Based Electrocatalysts via Optimizing the "Microparticles-in-Spider Web" Electrode Configurations. *Small* **2020**, *16* (8), 1–9. https://doi.org/10.1002/smll.201907029.

(17) Liu, D.; Ai, H.; Li, J.; Fang, M.; Chen, M.; Liu, D.; Du, X.; Zhou, P.; Li, F.; Lo, K. H.; Tang, Y.; Chen, S.; Wang, L.; Xing, G.; Pan, H. Surface Reconstruction and Phase Transition on Vanadium–Cobalt–Iron Trimetal Nitrides to Form Active Oxyhydroxide for Enhanced Electrocatalytic Water Oxidation. *Adv. Energy Mater.* **2020**, *10* (45), 1–9. https://doi.org/10.1002/aenm.202002464.

(18) Wang, Y.; Zhang, S.; Meng, X.; Wang, T.; Feng, Y.; Zhang, W.; He, Y. S.; Huang, Y.; Yang, N.; Ma, Z. F. Surface Tuning to Promote the Electrocatalysis for Oxygen Evolution Reaction: From Metal-Free to Cobalt-Based Carbon Electrocatalysts. *ACS Appl. Mater. Interfaces* **2021**, *13* (1), 503–513. https://doi.org/10.1021/acsami.0c17599.

(19) Hao, M.; Xiao, M.; Qian, L.; Miao, Y. Synthesis of Cobalt Vanadium Nanomaterials for Efficient Electrocatalysis of Oxygen Evolution. *Front. Chem. Sci. Eng.* **2018**, *12* (3), 409–416. https://doi.org/10.1007/s11705-017-1689-0.

(20) Chakrapani, K.; Bendt, G.; Hajiyani, H.; Lunkenbein, T.; Greiner, M. T.; Masliuk, L.; Salamon, S.; Landers, J.; Schlögl, R.; Wende, H.; Pentcheva, R.; Schulz, S.; Behrens, M. The Role of Composition of Uniform and Highly Dispersed Cobalt Vanadium Iron Spinel Nanocrystals for Oxygen

Electrocatalysis. *ACS Catal.* **2018**, *8* (2), 1259–1267. https://doi.org/10.1021/acscatal.7b03529.

(21) Liu, J.; Ji, Y.; Nai, J.; Niu, X.; Luo, Y.; Guo, L.; Yang, S. Ultrathin Amorphous Cobalt-Vanadium Hydr(Oxy)Oxide Catalysts for the Oxygen Evolution Reaction. *Energy Environ. Sci.* **2018**, *11* (7), 1736–1741. https://doi.org/10.1039/c8ee00611c.

(22) Cui, Y.; Xue, Y.; Zhang, R.; Zhang, J.; Li, X.; Zhu, X. Vanadium-Cobalt Oxyhydroxide Shows Ultralow Overpotential for the Oxygen Evolution Reaction. *Journal of Materials Chemistry A*. **2019**, pp 21911–21917. https://doi.org/10.1039/c9ta07918a.

(23) Liu, R.; Wang, Y.; Liu, D.; Zou, Y.; Wang, S. Water-Plasma-Enabled Exfoliation of Ultrathin Layered Double Hydroxide Nanosheets with Multivacancies for Water Oxidation. *Adv. Mater.* **2017**, *29* (30), 1–7. https://doi.org/10.1002/adma.201701546.

(24) Lv, J.; Liu, P.; Yang, F.; Xing, L.; Wang, D.; Chen, X.; Gao, H.; Huang, X.; Lu, Y.; Wang, G. 3D Hydrangea Macrophylla-like Nickel−Vanadium Metal−Organic Frameworks Formed by Self-Assembly of Ultrathin 2D Nanosheets for Overall Water Splitting. *ACS Applied Materials and Interfaces*. **2020**, pp 48495–48510. https://doi.org/10.1021/acsami.0c11722.